Arch. Metall. Mater. **70** (2025), 1, 335-340

DOI: https://doi.org/10.24425/amm.2025.152550

J. LIU[1,2*], J. LIU[3], X. WANG[3]

MICROSTRUCTURAL CHARACTERIZATION OF AS-CAST AND COLD DEFORMED PRECIPITATION STRENGTHENED Cu-3Ti-3Ni-0.5Si ALLOY

In this work, the microstructure and recrystallization behavior of Cu-3Ti-3Ni-0.5Si alloy after thermomechanical processing were investigated by light microscope (LM), scanning electron microscope (SEM), electron backscattering diffraction (EBSD), and transmission electron microscope (TEM). The results show that the as-cast Cu-3Ti-3Ni-0.5Si alloy consists of NiTi, Ni_3Si, Ni_2Si phases and Cu matrix, and the phase transformation occurs twice during the cooling process. Moreover, with increase of aging temperature, the precipitates in the Cu-3Ti-3Ni-0.5Si alloy matrix changes from rod-liked morphology to spherical shape, and the sizes and volume fraction of the spherical precipitates increase progressively. Furthermore, the number of the recrystallization grain increases with increase of the aging temperature, thus leading to decrease on the grain size. In addition, the fraction of low angle grain boundaries decreases, whereas the fraction of high angle grain boundary increases with increase of aging temperature.

Keywords: Copper alloy; aging; microstructure; precipitates; recrystallization

1. Introduction

Due to the excellent mechanical properties, good electrical and thermal conductivity, copper alloys have been widely used in computer technology, communication technology, the electrical devices, instrumentation, and precision machinery manufacturing [1-3]. Cu-Be alloy has high strength, excellent electrical conductivity, thermal conductivity, good fatigue, and corrosion resistance. Besides, no sparks are generated during the impact process. It has become an important material in modern industry. However, its production cost is relatively high, and toxic substances generated during manufacturing are detrimental to the humanity heath and environment. In addition, the elasticity and strength of Cu-Be alloy will drop sharply under working conditions above 150°C, and improper selection of Be content increases the brittleness of the alloy after solution aging treatment, resulting in poor toughness and fatigue properties of the Cu-Be alloy [4-6].

Cu-Ti alloys have high strength, good elasticity, good corrosion and wear resistance, and excellent high-temperature performance [7,8]. Besides, they have a wider service temperature range and a more straightforward production process, low cost, and abundant raw materials as compared to Cu-Be alloy. Therefore, it has become the ideal substitute of Cu-Be alloys [9,10]. However, the solid solution of Ti atoms in the Cu-Ti alloy matrix enhances the electron scattering. As a result, it substantially reduces the electrical conductivity of the Cu-Ti alloy, thereby limiting its applications [11]. Therefore, under the premise of not damaging the excellent mechanical properties of Cu-Ti alloys, how to improve the electrical conductivity has become an urgent problem in the development of Cu-Ti alloys with good comprehensive properties.

The electrical conductivity of Cu-Ti alloys can be increased by lowering the electron scattering, which can be achieved by reducing the amount of Ti solute atoms and alloying elements in the alloy. Based on this idea, alloying elements such as Sn [12], Cd [13], Cr [14], Co [15], P [16] and other elements are added to a Cu-Ti alloy. Nevertheless, the electrical conductivity of Cu-Ti alloys does not improve significantly. In our previous work [17], the microstructure and properties of Cu-3Ti-3Ni-0.5Si alloy were studied, but the microstructure change and recrystallization behavior of Cu-3Ti-3Ni-0.5Si alloy after thermomechanical processing are still unclear. To get in-depth insights of microstructure evolution and recrystallization behavior, the Cu-3Ti-3Ni-0.5Si alloy after thermomechanical processing were characterized by light microscope (LM), scanning electron microscopy (SEM),

[1] XI'AN POLYTECHNIC UNIVERSITY, SCHOOL OF MATERIALS SCIENCE AND ENGINEERING, XI'AN 710048, P.R. CHINA
[2] XI'AN UNIVERSITY OF TECHNOLOGY SCHOOL OF MECHANICAL AND PRECISION INSTRUMENT ENGINEERING, , XI'AN 710048, P. R. CHINA
[3] XI'AN UNIVERSITY OF TECHNOLOGY, SCHOOL OF MATERIALS SCIENCE AND ENGINEERING, XI'AN 710048, P. R. CHINA

* Corresponding author: liujia09200920@163.com)

electron backscattering diffraction (EBSD), and transmission electron microscopy (TEM) in this work. The purpose is gets insights of the solidification process of the Cu-3Ti-3Ni-0.5Si alloy and clarify its microstructure characteristics. The recrystallization behavior was characterized, and the correlation between recrystallization and heat treatment was disclosed. The research is of significance for the design of processing parameters of Cu-3Ti-3Ni-0.5Si alloy.

2. Experimental procedures

An alloy ingot (Cu-3Ti-3Ni-0.5Si (wt.%)) with 110×200 mm dimensions was fabricated in the vacuum induction melting furnace. After surface finishing, the as-cast ingot was homogenized at 800°C for 120 min in an electric resistance furnace. Next, the specimens with sizes of 120×50×10 mm were sliced from the ingot, and they were solution treated at 850°C for 240 min, followed by quenching in water. Afterwards, the specimens were cold-rolled with deformation of 50%, and subsequently aged for 120 min at temperatures ranging from 400 to 900°C, at the interval of 100°C. After being polished, the specimens were etched in a solution of 5 g $FeCl_3$, 15 mL HCl and 100 mL distilled water.

The morphology of the precipitated phases was characterized using a GX71 light microscope (LM), a Zeiss-Merlin scanning electron microscope (SEM) equipped with an Oxford Instruments HKL channel 5 electron backscattering diffraction (EBSD), and a JEM-3010 transmission electron microscope (TEM). The EDS mapping was performed on the Zeiss-Merlin scanning electron microscope to analyze the distribution of elements. EBSD data was acquired at the scanning step size of 0.6 μm. The specimen was tilted 70° for EBSD mapping at the acceleration voltage of 20 kV. The samples for EBSD analysis were prepared by mechanical polishing with subsequent vibratory polishing for 30 min. A JEM-3010 transmission electron microscope was used to observe the microstructures with an operating voltage of 200 kV. The specimens used for TEM observations were cut from the block using a Somet1000 precision saw and then mechanically polished to obtain 50 μm thick slices. Discs of 3 mm diameter were punched from these slices and thinned in a Fischione1010 ion milling machine at 4.5 kV.

3. Results and discussion

3.1. As-cast microstructure

The microstructure of the as-cast Cu-3Ti-3Ni-0.5Si alloy at different magnifications under the LM is displayed in Fig. 1. As seen from Fig. 1, the as-cast Cu-3Ti-3Ni-0.5Si alloy presents the dendrite structure.

Fig. 2 represents the SEM image and EDS mapping results. Apparently, the coarse primary phase is continuous between dendrites (Fig. 2(a)), and the fine irregular spherical and short rod primary phase appears (Fig.2(b)). To observe the distribution

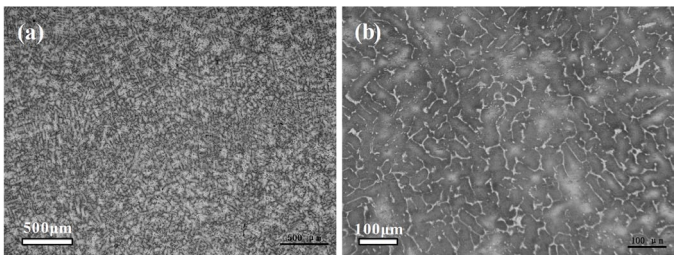

Fig. 1. Microstructure of as-cast Cu-3Ti-3Ni-0.5Si alloy at low (a) and high (b) magnification

of elements of the as-cast Cu-3Ti-3Ni-0.5Si alloy, the element mapping analysis was conducted by EDS, and the results are shown in Figs. 2(c)-(f).

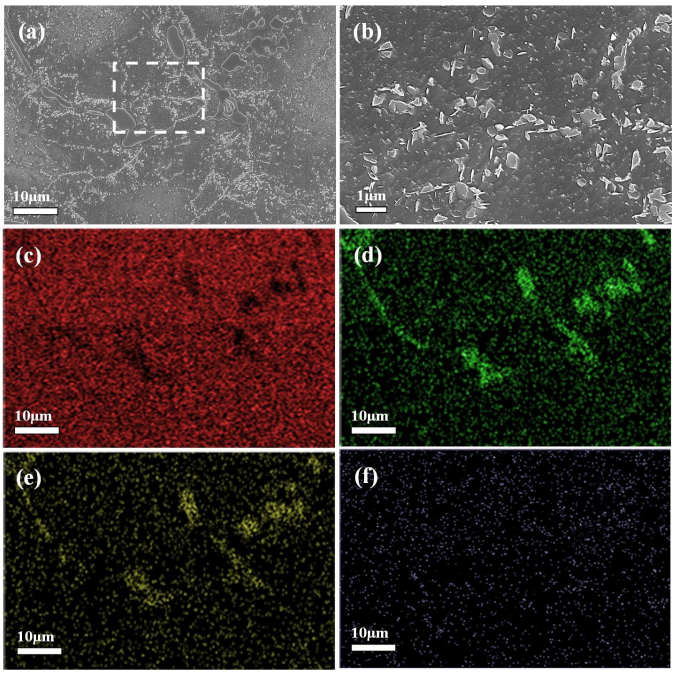

Fig. 2. The map analysis of as-cast Cu-3Ti-3Ni-0.5Si alloy: (a) mapping area; (b) magnified micrograph of (a); (c) Cu element; (d) Ti element; (e) Ni element; (f) Si element

It can be seen that the as-cast Cu-3Ti-3Ni-0.5Si alloy matrix is mainly composed of Cu, and the Cu content is shallow in the second phase particles of non-equilibrium solidification, as shown in Fig. 2(c). The second phase of non-equilibrium solidification is composed of Ni and Ti (Fig. 2(d)-(e)). In addition, Si is uniformly distributed in the copper matrix (Fig. 2(f)).

To further clarify the phase constituents, TEM analysis was performed on the as-cast Cu-3Ti-3Ni-0.5Si alloy, as shown in Fig. 3. Fig. 3(a) is the TEM image, and Fig. 3(b) is the selected area electron diffraction pattern (SAED) with an electron beam along the zone axis of $[10\bar{1}]$. From Fig. 3(a), it can be observed that the size of irregular particles is about 1 μm. As determined from the selected area electron diffraction pattern (SAED), the irregular particles are NiTi phase, which has a monoclinic structure with the lattice parameters a = 0.2885 nm, b = 0.4622 nm, c = 0.412 nm, a = 90°, b = 96.8°, g = 90°. Fig. 3(c) is the TEM

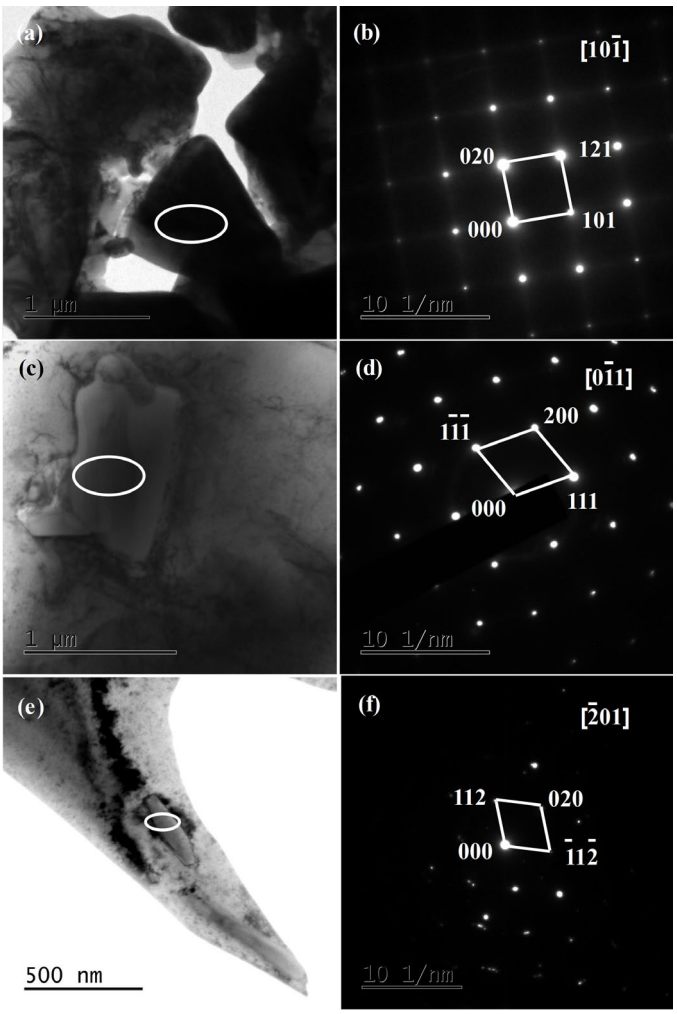

Fig. 3. TEM images (a, c, e) and corresponding SAED patterns (b, d, f) of as-cast Cu-3Ti-3Ni-0.5Si alloy

image, and Fig. 3(d) is the selected area electron diffraction pattern (SAED) with an electron beam along the zone axis of [0$\bar{1}$1], it can verify that the precipitation phase is Ni_3Si, which has a cubic structure with the lattice parameters a = 0.3506 nm, b = 0.3506 nm, c = 0.3506 nm, a = 90°, b = 90°, g = 90°. In addition, it can observe striped precipitates from Fig. 3(e). As determined from the SAED pattern, the striped precipitate is Ni_2Si phase, which has an orthogonal structure with the lattice parameters a = 0.499 nm, b = 0.372 nm, c = 0.703 nm, a = 90°, b = 90°, g = 90°, as seen from Fig. 3(f).

To determine the temperature of phase transformation, the differential thermal analysis (DSC) analysis was performed on the as-cast Cu-3Ti-3Ni-0.5Si alloy, and the result is shown in Fig. 4(a). Fig. 4(b) is an enlarged view of the dotted line on the cooling curve of Fig. 4(a). From Fig. 4, two endothermic peaks occur during the heating process, while two exothermic peaks appear during the cooling process of the alloy, indicating twice phase transformation during the cooling process. From Fig. 4(b), the first phase transformation occurs at 1070°C, which is close to the melting point of pure copper at 1083°C. Therefore, it can be inferred that the first phase transformation is essential for forming the Cu-rich phase while various primary phases are formed. Furthermore, it can be seen from the cooling curve that with the decrease of temperature, the corresponding temperature of the second phase transformation is 1061°C, and the second phase transformation temperature shown in the alloy cooling curve is lower than that of the melting point of NiTi phase. Therefore, it can be explained that when the second phase transformation occurs, the primary phase generates a Cu-rich phase and NiTi phase [18]. Combined with TEM analysis, it can be seen that for the as-cast alloy, the NiTi is the primary phase because Ni_3Si and Ni_2Si phases are precipitated in the Cu-rich phase.

3.2. Recrystallization behavior

To clarify the effect of aging temperature on microstructure, SEM analysis was conducted on the cold-rolled specimens after ageing at different temperatures for 120 min, and the results are presented in Fig. 5. As seen from Fig. 5, these precipitation phases present different sizes and morphologies. In our previous work, these precipitation phases were analyzed, and more details can refer to the literatures [17]. After aging 400°C, irregular particles and numerious rod-shaped particles precipitate, see Fig. 5(a). With increase of aging temperature, the precipitates changes from rod-like morphology to spherical shape, and the size of spherical precipitates increases progressively (Figs. 5(b)-(e)).

To further disclose the precipitation behavior, TEM analyses were performed on the cold-rolled after aging at 500, 600, 700, and 800°C for 120 min, and the TEM analysis results are displayed in Fig. 6. After aging at 500°C, the fine second phase has rod-like shape (Figs. 6(a)), while the fine second phase presents finely granular morphology after aging at 600°C (Fig. 6(b)).

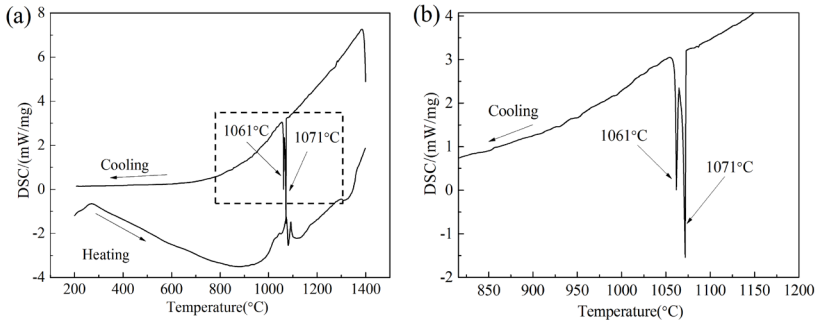

Fig. 4. The DSC curves of as-cast Cu-3Ti-3Ni-0.5Si alloy (a) and enlarged cooling curve (b)

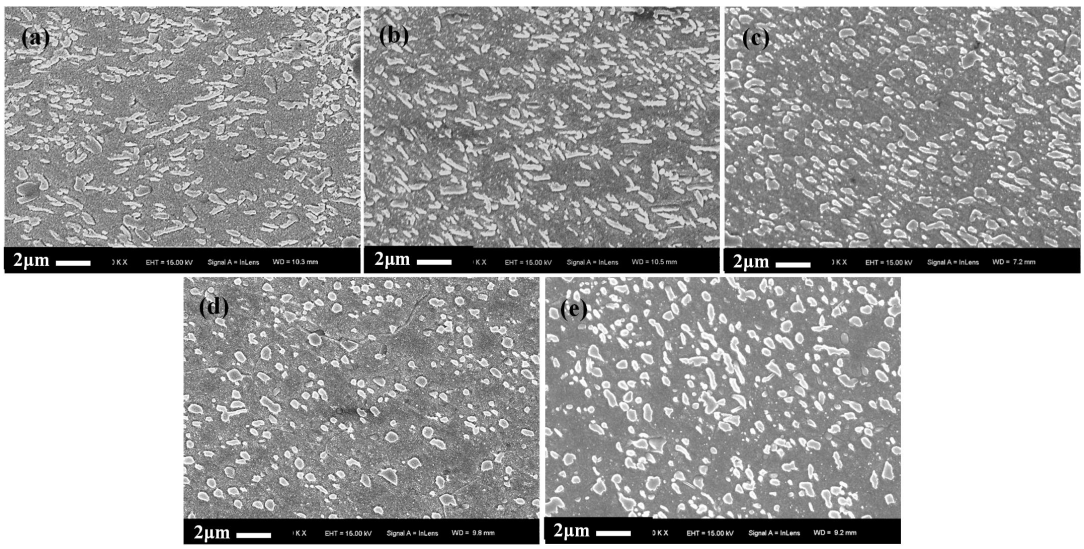

Fig. 5. SEM micrographs of the cold-rolled Cu-3Ti-3Ni-0.5Si alloy after aging at different temperatures for 120 min: (a) 400°C; (b) 500°C; (c) 600°C; (d) 700°C; (e) 800°C

In addition, the volume fraction of precipitates is relatively small. Several studies believed that these second phase precipitated at the grain boundary can hinder the recrystallization of the alloy [19-22]. With further increase of aging treatment, both the size and volume fraction of precipitates increases significantly (Fig. 6(c) and Fig. 6(d)). Generally, the second phase firstly precipitated at the subgrain boundary and dislocation hinders the movement of subgrain and dislocation, resulting in recrystallization [23-25]. Deformation leads to the increase of dislocation density at the interface between the second precipitate and the matrix, giving rise to a high-density dislocation stacking around the precipitate, which is conducive to the nucleation and growth of recrystallization [25].

To better understanding the change of recrystallization after aging, the cold-rolled Cu-3Ti-3Ni-0.5Si alloy after aging at 700 and 800°C for 120 min were analyzed by EBSD, the EBSD results are presented in Fig. 7 and Fig. 8. From Fig. 7, it can clearly observe the recrystallization grains, and the number of the recrystallization grain increases with increase of the aging temperature.

The grain size distribution and grain boundary misorientation distribution of cold-rolled Cu-3Ti-3Ni-0.5Si alloy after aging at 700 and 800°C for 120 min are illustrated in Fig. 8. It can be seen from Figs. 8(a) and 8(b) that the grain size decreases with increase of aging temperature, which is caused by a large amount of recrystallization [24,25]. In addition, the low

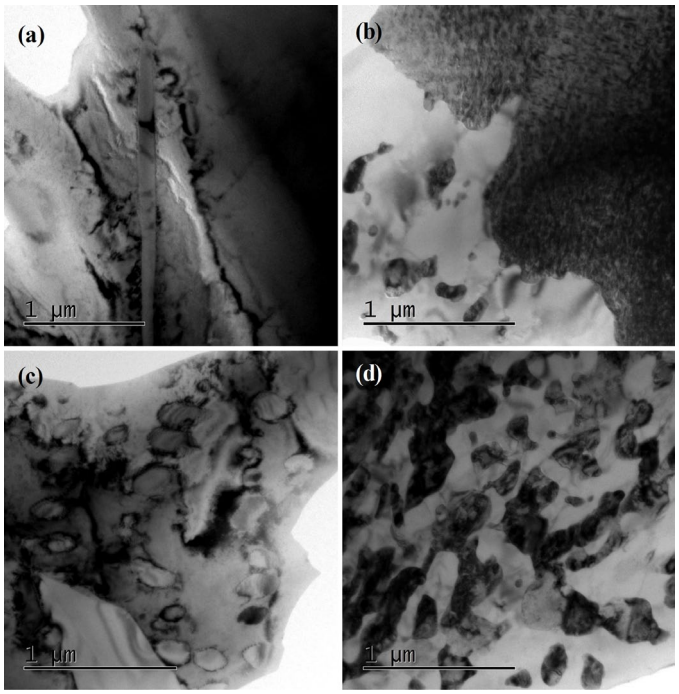

Fig. 6. TEM images of the cold-rolled Cu-3Ti-3Ni-0.5Si alloy after aging at different temperatures for 120 min: (a)500°C; (b) 600°C; (c)700°C; (d) 800°C

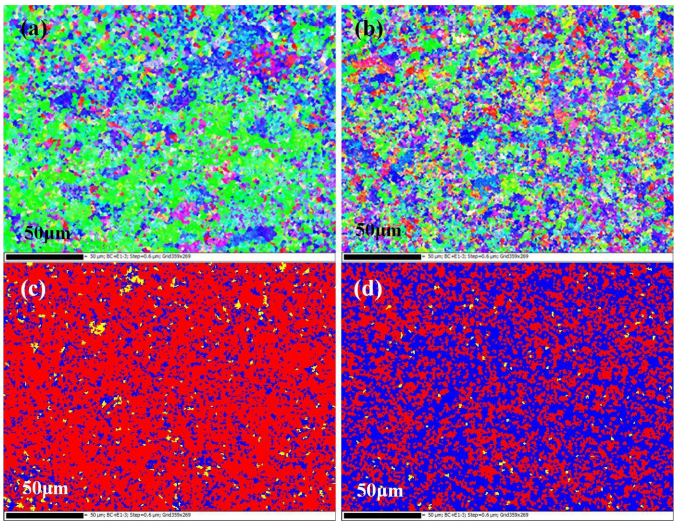

Fig. 7. Orientation mappings (a, b) and recrystallization grains distribution (c, d) of cold-rolled Cu-3Ti-3Ni-0.5Si alloy after aging at 700°C (a, c), 800°C (b, d) for 120 min (blue, yellow and red color represent recrystallization, subgrain and deformed zone, respectively)

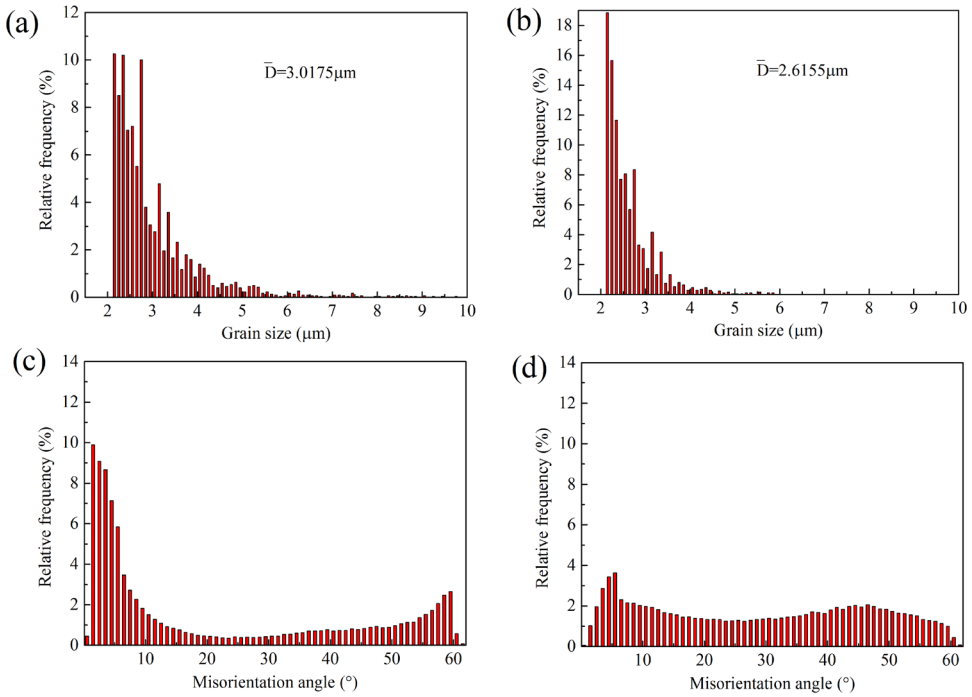

Fig. 8. Grain size distribution (a, b) and grain boundary misorientation distribution (c, d) of cold-rolled Cu-3Ti-3Ni-0.5Si alloy after aging at 700°C (a, c), 800°C (b, d) for 120 min

angle grain boundaries decrease, whereas the high angle grain boundaries increase with increasing aging temperature (Fig. 8(c) and Fig. 8(d)). From study by Humphreys et al. [23], small-sized subgrains are merged with large-sized subgrains into a grain due to the rotation of subgrain boundaries, which increases the misorientation between the large-sized subgrains and adjacent subgrains, thereby resulting in the formation of the high-angle grain boundaries, which further promotes the nucleation of recrystallization.

4. Conclusions

In this study, the microstructure and recrystallization behavior of Cu-3Ti-3Ni-0.5Si alloy after solution treatment, cold rolling and aging at different temperatures were characterized and analyzed. The main findings and conclusions can be summarized as follows.

1) The as-cast Cu-3Ti-3Ni-0.5Si alloy is mainly consisted of NiTi, Ni_3Si, Ni_2Si phases.
2) The first phase transformation occurs at 1070°C, the second phase transformation generates at the temperature of 1061°C during the cooling process.
3) With increase of aging temperature, the precipitates changes from rod-like morphology to spherical shape, and the sizes and volume fraction of the spherical precipitates increase progressively.
4) The increased aging temperature decreases the fraction of low angle grain boundaries, but increases the fraction of high angle grain boundaries, resulting in the decreased grain size.

Acknowledgment

This research was supported by the Natural Science Basic Research Program of Shaanxi Province (No. 2023-JC-QN-0550), Science and Technology Guidance Program Project of China National Textile and Apparel Council (No. 2021039)

REFERENCES

[1] T. Kunimine, Y. Tomaru, M. Watanabe, R. Monzen, Mater. Trans. **62**, 479-483 (2021).
DOI: https://doi.org/10.2320/matertrans.MT-M2020308
[1] B.M. Luo, D.X. Li, C. Zhao, Z. Wang, Z.Q. Luo, W.W. Zhang, Mater. Sci. Eng. A **746**, 154-161 (2019).
DOI: https://doi.org/10.1016/j.msea.2018.12.120
[2] Y.X. Liu, L. Wang, K. Jiang, S.T. Yang, J. Alloys Compd. **775**, 818-825 (2019).
DOI: https://doi.org/10.1016/j.jallcom.2018.10.207
[3] Y.J. Zhou, K.X. Song, J.D. Xing, Y.M. Zhang, J. Alloys Compd. **658**, 920-930 (2016).
DOI: https://doi.org/10.1016/j.jallcom.2015.10.290
[4] A.I. Morozova, A.N. Belyakov, R.O. Kaibyshev, Phys. Met. Metallogr. **122**, 60-66 (2021).
DOI: https://doi.org/10.1134/S0031918X21010087
[5] Y.J. Zhou, K.X. Song, X.J. Mi, Y. Liu, S.D. Yang, Z. Li, Rare. Metal. Mat. Eng. **47**, 1096-1099 (2018).
DOI: https://doi.org/10.1016/S1875-5372(18)30126-7
[6] M.Z. Ma, Z. Li, W.T. Qiu, Z. Xiao, Z.Q. Zhao , Y.B. Jiang, J. Alloys Compd. **788**, 50-60 (2019).
DOI: https://doi.org/10.1016/j.jallcom.2019.01.335

[7] R. Li, X.W. Zuo, E.G. Wang, J. Alloys Compd. **773**, 121-130 (2019). DOI: https://doi.org/10.1016/j.jallcom.2018.09.179

[8] B. Rouxel, C. Cayron, J. Bornand, P. Sanders, R.E. Logéa, Mater. Design. **213**, 110340 (2022). DOI: https://doi.org/10.1016/j.matdes.2021.110340

[9] M. Sobhani, A. Mirhabibi, H. Arabi, R.M.D. Brydson, Mater. Sci. Eng. A **577**, 16-22 (2013). DOI: https://doi.org/10.1016/j.msea.2013.03.063

[10] A.A. Eze, T. Jamiru, E.R. Sadiku, M.O. Durowoju, W.K. Kupolati, I.D. Ibrahim, B.A. Obadele, P.A. Olubambi, S. Dioufbf, J. Alloys Compd. **736**, 163-171 (2018). DOI: https://doi.org/10.1016/j.jallcom.2017.11.129

[11] Y.F. Geng, Y.J. Ban, X. Li, Y. Zhang, Y.L. Jia, B.H. Tian, M. Zhou, Y. Liu, A.A. Volinsky, K.X. Song, S.L. Tang, Mater. Sci. Eng. A **821**, 141639 (2021). DOI: https://doi.org/10.1016/j.msea.2021.141639

[12] X.H. Wang, C.Y. Chen, T.T. Guo, J.T. Zou, Y.H. Yang, J. Mater. Eng. Perform. **24**, 2738-2743 (2015). DOI: https://doi.org/10.1007/s11665-015-1483-4

[13] R. Markandeya, S. Nagarjuna, D.V.V. Satyanarayana, D.S. Sarma, Mater. Sci. Eng. A, **428**, 233-243 (2006). DOI: https://doi.org/10.1016/j.msea.2006.05.034

[14] X. Wang, Z. Xiao, W.T. Qiu, Z. Li, F. Liu, Mater. Sci. Eng. A **803**, 140510 (2021). DOI: https://doi.org/10.1016/j.msea.2020.140510

[15] H.Y. Yang, Y.Q. Bu, J.M. Wu, Y.T. Fang, J.B. Liu, H.T. Wang, W. Yang, Mater. Charact. **176**, 111099 (2021). DOI: https://doi.org/10.1016/j.matchar.2021.111099

[16] S. Kim, M. Kang, J. Ind. Eng. Chem .**18**, 969-978 (2012). DOI: https://doi.org/10.1016/j.jiec.2011.10.009

[17] J. Liu, X.H. Wang, J. Chen, J.T. Liu, J. Alloys Compd. **797**, 370-379 (2019). DOI: https://doi.org/10.1016/j.jallcom.2019.05.091

[18] H. Yoon-Uk, T. Masaki, F. Kazuo, L. Hu-Chul Lee, Acta Mater. **57**, 1176-1187 (2009). DOI: https://doi.org/10.1016/j.actamat.2008.10.056

[19] X.Y. Yang, H. Miura, T. Sakai, T. Nonferr. Metal. Soc. **17**, 1139-1142 (2007). DOI: https://doi.org/10.1016/S1003-6326(07)60239-8

[20] Y.F. Shi, C.J. Guo, J.S. Chen, X.P. Xiao, H. Huang, B. Yang, Mater. Sci. Eng .A **826**, 142025 (2021). DOI: https://doi.org/10.1016/j.msea.2021.142025

[21] Q.C. Ma, J.Y. Ma, J.L. Zhou, H.J. Jia, J .Mater. Res. Technol. **17**, 353-364 (2022). DOI: https://doi.org/10.1016/j.jmrt.2022.01.011

[22] F.J. Humphreys, Acta Metall. **25** (11), 1323-1344 (1977). DOI: https://doi.org/10.1016/0001-6160(77)90109-2

[23] Z. Shen, Z.Z. Lin, P.J. Shi, G.P. Tang, T.X. Zheng, C.M. Liu, Y.F. Guo, Y.B. Zhong, Mater. Sci. Eng. A **820**, 141548 (2021). DOI: https://doi.org/10.1016/j.msea.2021.141548

[24] C. Zhao, Z. Wang, D.Q. Pan, D. X. Li, Z.Q. Luo, D.T. Zhang, C. Yang, W.W. Zhang, T. Nonferr. Metal. Soc. **29** (12), 1139-1142 (2019). DOI: https://doi.org/10.1016/S1003-6326(19)65163-0

[25] N. Xu, L. Chen, R.N. Feng, Q.N. Song, Y.F. Bao, J. Mater. Res. Technol. **9** (3), 3746-3758 (2020). DOI: https://doi.org/10.1016/j.jmrt.2020.02.001